Advanced Materials Science

Research Article

Synthesis, characterization of Cu, N co-doped TiO_2 microspheres with enhanced photocatalytic activities

Honghong Liu[1], Mingming Zou[1,2], Branislav Viliam Hakala[1,3], Rasaki Sefiu Abolaji[1] and Minghui Yang[1]*

[1]Ningbo Institute of Industrial Technology, Chinese Academy of Sciences, No. 1219 Zhongguan West Road, Zhenhai District, Ningbo, China

[2]Dalian Institute of Chemical Physics, Chinese Academy of Sciences, Dalian 116023, P R China

[3]Institute of Physics, Faculty of Science, P.J. Šafárik University, Park Angelinum 9, SK-04154 Košice, Slovakia

Abstract

The mesoporous Copper, nitrogen co-doped TiO_2 microspheres was prepared via solvothermal approach, followed by nitriding treatment under an ammonia gas flow. The crystalline structures of the as-prepared catalyst and the chemical compositions of Cu,N co-doped TiO_2 were determined using X-ray diffraction (XRD) and X-ray photoelectron spectroscopy (XPS) respectively. The photocatalytic activity of the as-prepared sample was investigated by monitoring the degradation of Rhodamine-B under visible light irradiation.

Experimental results indicated that mesoporous Cu,N co-doped TiO_2 microspheres showed higher photocatalytic activity than Cu-TiO_2 microspheres and anatase TiO_2 under visible light irradiation. The higher photocatalytic activity of the mesoporous Cu,N co-doped TiO_2 microspheres sample could be attributed to the synergistic effects of large BET surface area, extended light absorption, efficient charge separation which was stabilized by the presence of oxygen vacancies. It was discovered that, valence states maintain stability after nitriding treatment. The sample synthesized from 0.1% molar quantity of Cu dopant, and nitrided at 400℃ for 30 min gave the highest photocatalytic activity.

Introduction

Titanium dioxide (TiO_2) nanomaterials are the most widely used semiconductor in many applications such as energy storages, sensors, photovoltaics and photo-catalysis [1] because of its unique photo-electric properties, high chemical stability, low cost and environmental friendly [2-6]. However, photo-catalytic performance of TiO_2 is relatively low due to fast recombination of electron-hole pairs and narrow light response range [7] compare to noble metal modified TiO_2 which has been proved to be very effective in overcoming this drawback [8-10]. Since the lower Fermi level of noble metals resulting in an efficient separation of charge carriers, enhanced performance of photocatalysis could be achieved. However, noble metals are expensive and rare; hence, identification of metals with similar enhancement for photo-catalytic activity increasingly draws research attentions. Cu is much cheaper compared to noble metals, and Cu-TiO_2 has been extensively studied for the photodegradation of organic pollutants [11-14]. The electrons generated from the excitation of photocatalyst in the valence band (VB) of TiO_2 are directly transferred to Cu^{2+} under conduction band, which frees up the oxidative valence hole of the photocatalyst for the degradation of organic compounds. Metal ion dopants can serve as charge trapping sites and thus reduce electron-hole recombination rate during photocatalysis [15].

Recent years, many researchers also pay attention to dope TiO_2 with non-metals such as S, N, P and B [16-21]. Among all the non-metals-doped TiO_2 catalysts, N-doped TiO_2 had been intensively investigated. The N-doped pathway could form intermediate energy levels in the band gap as a consequence of either mixing N 2p with O 2p states or by introducing localized states. Comparing with single doping, co-doping of metal(s) and non-metal(s) on TiO_2 shows better performances in photocatalysis due to the synergetic effects [22-24] of large BET surface area and extended light absorption.

In our research work, we reported mesoporous Cu,N co-doped TiO_2 microspheres that showed relatively high catalytic activity. Here, we present a green solvothermal approach for the synthesis of mesoporous Cu doped TiO_2 microspheres. Nitrogen was doped on Cu-TiO_2 microspheres by nitriding treatment under an ammonia gas flow. The as-prepared sample could efficiently overcome the drawbacks mentioned above to some extent, because it has high sufarce area, effective charge separation and ability to absorb light at visible light region. Mesoporous structures with high surface area can provide an excellent support for active sites due to pore sizes and volume. Photocatalytic activity of the as-prepared catalyst was investigated by monitoring the degradation of Rhodamine-B (RhB) under visible light irradiation.

Experimental section

Materials and methods

All chemicals were analytical grade reagents and used without further purification. Hexadecylamine (HDA; 90%), Titanium (IV)

Correspondence to: Minghui Yang, Ningbo Institute of Industrial Technology, Chinese Academy of Sciences, No. 1219 Zhongguan West Road, Zhenhai District, Ningbo, 315201 China, Tel/Fax: +86-411-85168242, E-mail: myang@nimte.ac.cn

Key words: *Visible light photo-catalysis, TiO_2, nanostructure, nitridation, co-doping, photodegradation*

Received: January 02, 2017; **Accepted:** January 27, 2017; **Published:** January 30, 2017

isopropoxide (TIP; 98%), Copper chloride ($CuCl_2$), absolute ethanol, deionized water, potassium chloride(AR) and anatase TiO_2 were supplied by the Sigma-Aldrich, China. Rhodamine-B was used as model organic pollutant to evaluate the photocatalytic activity of the synthesized materials, and double distilled water was used throughout the experiment.

Synthesis of mesoporous Cu-doped TiO_2 microspheres (Cu-TiO_2): Mesoporous Cu-TiO_2 microspheres were synthesized *via* solvothermal reaction of TIP, HDA, KCl, and $CuCl_2$, followed by calcination. Firstly, mixture of $CuCl_2$ and TIP in molar ratios: 0.01, 0.02, 0.05, 0.1, 0.5, 1, 3, and 10, 1.98 g HDA and 1.60 mL of 1.6 M KCl solution were dispersed in 200 mL ethanol under stirring and the sample was allowed to react for 30 min. TIP (4.5 mL) as Titanium source was slowly dripped into the mixture under stirring. After 2 min, the white precursor bead in suspension was kept static for 18 h, centrifuged and washed with ethanol three times, and the sample was then air-dried at room temperature. After that, the sample was transferred into a Teflon-lined autoclave with a capacity of 100 mL. The autoclave was sealed, transferred to electric muffle furnace and kept at 160°C for 6 h. The precipitate obtained was collected by the centrifugation, washed with ethanol and air-dried. Finally, these powders obtained were calcined at 500°C for 2 h leading to the formation of Cu-TiO_2 microspheres. In this research work, TiO_2:(0.1 at% Cu) stands for 0.1 at % Cu loaded TiO_2 sample wherein the % is to be interpreted in terms of the molar ratio mentioned earlier in this paragraph.

Synthesis of Mesoporous Cu, N Co-doped TiO_2 microspheres (Cu-N-TiO_2): The sample obtained TiO_2:(0.1 at% Cu) was placed in a quartz boat. The boat was placed in a quartz tube with airtight, stainless steel end-caps that have welded valves and connections to input and output gas lines. The quartz tube was placed in a tube furnace and appropriate connection to the gas sources was made. An argon gas was allowed to flow through the tube for 15 min to expel air in the tube before establishing the flow of ammonia gas through the tube. The sample was then heated in the tube at 400°C, 500°C and 600°C with heating rate 4°C/min. After 30 min or 2 h elapsed, the furnace was turned off and the product was cooled to room temperature within 4 h under ammonia gas flow. Before the quartz tube was taken out of the tube furnace, argon gas was allowed to flow through the tube in order to expel the remaining ammonia gas in the tube. In this research work, TiO_2:(0.1 at% Cu,N - T - t) stands for 0.1 at % Cu doped TiO_2 with nitriding treatment time t = 30 min or 2 h and calcined at T = 400, 500 and 600°C.

Characterization

The crystalline structures of the sample was examined with X-ray diffraction (XRD) using X-ray Diffraction (XRD) with Miniflex600 X-ray diffractometer containing monochromatic Cu Kα radiation (λ=0.1542 nm, accelerating voltage 40 kV, applied current 15 mA) at scanning rate of 1°/min. The morphology and chemical composition were determined using scanning electron microscopy (SEM) instrument (JSM-7800F, Japan) and X-ray Photoelectron Spectroscopy (XPS) respectively. XPS measurements were carried out on an X-ray photoelectron spectrometer (ESCALAB250Xi) using Al Kα (1486.6 eV) X-rays as the excitation source. Carbon 1s (284.6 eV) was chosen as reference. UV-vis diffuse reflectance spectra were recorded with a Hitachi U-3900 spectrometer in the range of 200-850 nm, using $BaSO_4$ standard as reference. Surface area measurements were carried out by using nitrogen adsorption-desorption technique of Brunauer-Emmet-Teller (BET) method on Accelerated Surface Area and Porosimetry System (ASAP 2420) to obtain value of specific surface area, pore volumes and mean value of pore sizes.

Determination of photocatalytic properties and degradation of Rhodamine-B (RhB)

Photocatalytic properties were determined in an open thermostatic photo-reactor. Before light irradiation, 200 mL of suspension solution containing 10 mg/L RhB and 120 mg solid catalyst was sonicated for 10 min, and then stirred for 1 h in the darkness to ensure an adsorption–desorption equilibrium was maintained. The suspension was then irradiated under continuous stirring using UV light, 300 W Micro-solar 300UV - Xe lamp with a UV-cut off filter and was positioned 25 cm away from the reactor (removing the effect of light on the photocatalysis) in order to allow only visible light in the range of 420 nm-850 nm to interact with the sample, and the experiment was carried out at 25°C under constant stirring. At a given time, interval of irradiation, 5 mL of the solution was withdrawn, centrifuged and analysis with a UV-vis absorption (Hitachi U-3900 spectrometer) at the maximal absorption wavelength for RhB, which have characteristic absorption peaks of 554 nm (λ_{RhB}). To establish the stability of the photocatalyst, the mesoporous Cu-N-TiO_2 spheres was recycled and used three times for testing subsequent photocatalytic activities as follows; After a photocatalytic experiment, the mesoporous Cu-N-TiO_2 microspheres was recovered by washing with distilled water three times and dried at 80°C for 12 h to remove the residual reactants and reactivated the adsorption and catalytic performance.

Results and discussion

Crystal phases and morphology of the Cu-TiO_2 microspheres

Crystalline phases of the samples with different molar mass of Cu^{2+} were investigated with XRD, as shown in Figure S1. All the diffraction peaks are index to anatase TiO_2 structure (JCPDS card NO.21-1272) with five main characteristic peaks; the planes (101), (004), (200), (105) and (211) respectively. No impurity was detected except in 10 at% Cu-TiO_2 sample, and this indicated that copper dopant has a negligible effect on the crystalline phases of TiO_2 microspheres. The diffractograms of all the samples were not shown any diffraction peaks of copper or copper compounds except the one of 10% Cu-TiO_2 which could be attributed to low copper content in these samples. In the present study, the Cu is in +2 oxidation state and Ti is in +4 oxidation state. The radius of Ti^{4+} (0.68 Å) is similar to that of Cu^{2+} (0.73 Å), hence copper ions may be incorporated into the lattice of TiO_2 and occupied some of the titanium lattices [25,26]. The charge compensation is mainly achieved by the ionized vacancies especially doubly ionized oxygen vacancies. As shown in Figure 2, in order to further enhance the photocatalytic activity of TiO_2: (0.1 at% Cu) sample in the visible light region, nitriding treatment were carried out under ammonia gas flow. The PXRD patterns of TiO_2:(0.1 at% Cu, N-400°C-30 min) sample shows a good crystallinity, and the PXRD patterns of mesoporous TiO_2:(0.1 at% Cu, N) microspheres with different nitriding conditions are shown in Figure S2.

All the samples exhibit good crystallinity of anatase TiO_2 diffraction peaks (JCPDS no. 21-1272) with no other peaks, demonstrating phase purity, because the temperature and time of nitriding treatment were not sufficient to produce TiN.

Figure 3 shows the scanning electron microscopy (SEM) images (morphology) of the synthesized Cu-TiO_2, and Figure 3A, B show the typical FESEM images of the as-synthesized mesoporous TiO_2:(0.1 at%

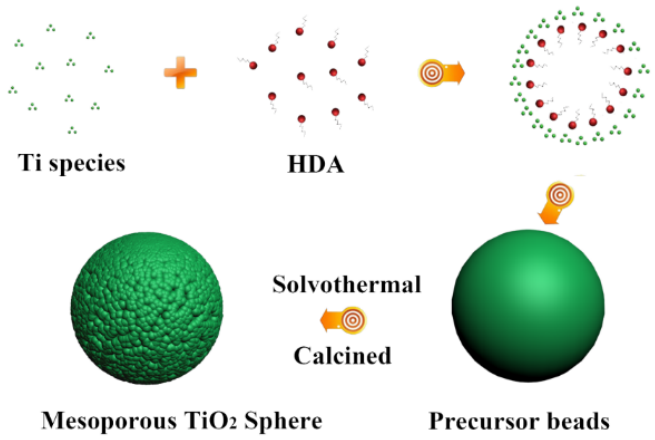

Figure 1. possible mechanism for beads growth.

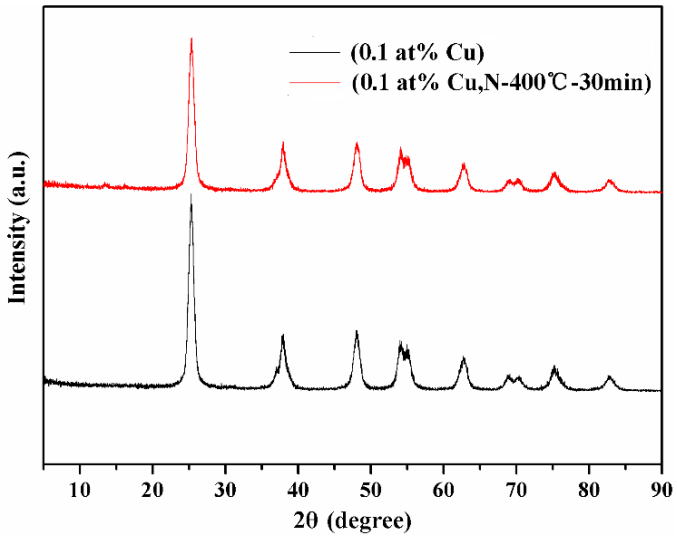

Figure 2. XRD patterns of TiO_2: (0.1 at% Cu) and TiO_2: (0.1 at% Cu, N-400°C-30 min) microspheres.

Cu) microspheres at different magnifications. During calcinations, monodispersed TiO_2:(0.1 at% Cu) microspheres with a diameter of (0.6 ± 0.05) μm, and comparatively rough surfaces are produced (Figure 3A) owing to the removal of the template. As illustrated by the high magnification SEM image (Figure 3B), TiO_2 beads contain nanocrystals and pores were obviously observed over the surface of the beads. This special structure is beneficial by allowing light scattering on the surface and in the pores of the beads. Even after nitriding treatment at 500°C for 2 h, agglomeration of TiO_2:(0.1 at% Cu, N-500°C-2 h) was not obvious, and some microspheres were broken. However, the beads still retained mesoporous structures as shown in Figure 3C, D.

The EDS spectrum (Figure 3E) indicated that the composite consists of Cu, Ti and O as it was revealed by EDS technique. Moreover, the elemental mapping of TiO_2:(3 at% Cu) was also performed by EDS area scanning and amount of Cu present was too low to be detected. So, we choose a relative high Cu content sample (3 at% Cu) in order to estimate amount of copper present in the sample by using EDS. The maps (Figure 3F, G and H) of O, Ti, and Cu are well defined with sharp contrast, and the profile of Cu is close to that of O and Ti, which indicates that Cu and Ti are distributed uniformly and densely

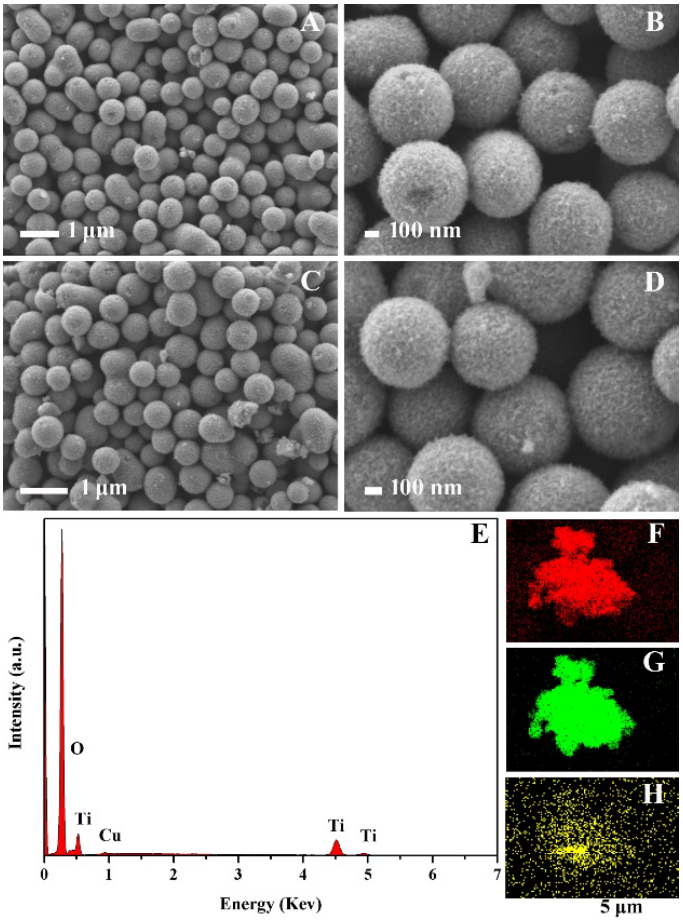

Figure 3. Typical FESEM (A and B) of TiO_2: (0.1 at% Cu) and (C and D) of TiO_2:(0.1 at% Cu, N-500°C-2 h) samples, EDS mapping (E, F(O), G(Ti) and H(Cu)) images of TiO_2: (3 at% Cu) sample.

throughout the whole composite.

BET surface area and pore size distribution of the Cu-TiO_2 microspheres

To examine the porosity of the TiO_2:(0.1 at% Cu) and TiO_2:(0.1 at% Cu, N-500°C-2 h), N_2 adsorption-desorption isotherms were performed, and results obtained are shown in Figure S3. The corresponding mono-modal pore-size distributions (inset, Figure S3) indicates the mesoporous nature of the two samples with the pore sizes smaller than 10 nm, and after nitriding treatment the pores were almost not changed. As a result, the mesoporous TiO_2:(0.1 at% Cu) microspheres has a high BET surface area of 113.3 m^2g^{-1} owing to the presence of mesoporous nature. Furthermore, after nitriding treatment under ammonia gas, the as-prepared TiO_2:(0.1 at% Cu, N-500°C-2 h) sample was also investigated using BET technique, and it is important to note that surface area of the sample is 109.4 m^2g^{-1} and there was no significant decrease in the value except a slight change after nitriding treatment, which might due to the nitriding temperatures. It was discovered from results that all obtained Cu-TiO_2 microspheres have excellent surface and mesoporous properties, which might lead to high photocatalytic activities.

Formation process of Cu-TiO_2 microspheres

Figure 1 shows a schematic diagram of a possible mechanism for the beads growth process. Based on these results, we propose that

the formation of mesoporous spheres proceeds through keeping static, solvothermal and calcination reaction. The mesostructures and monodisperse precursor beads were formed through a cooperative assembly process involving long-chain alkylamine and $Ti(OCH(CH_3)_2)_{4-x}(OH)_x$ species. The resultant $Ti(OCH(CH_3)_2)_{4-x}(OH)_x$ species on hydrolysis of Titanium (IV) isopropoxide (TIP) participate in hydrogen-bonding interactions with amino groups of the Hexadecylamine (HDA), such hybrid composites contain hydrophobic long-chain of alkyl groups. Meanwhile, further hydrolysis and condensation of the titanium species associated with the hybrid micelles resulted into the formation of a new liquid condensed phase rich in HDA which can be referred to as titanium oligomers. As the titanium oligomers further polymerized, the condensed phase became denser, and this might due to effect of ammonia released during hydrolysis hastening decomposition of titanium oligomers leading to the formation of mesostructured inorganic frameworks which finally precipitated out of the solvent. During solvothermal treatment, amorphous TiO_2 was known to experience a phase change to anatase via a dissolution and reprecipitation processes, wherein dissolved titanate species rapidly nucleated to form nanocrystalline structures due to the high solvothermal system. Further calcination in air induces decomposition of HDA molecules and promotes the formation of well crystalline mesoporous TiO_2 sphere.

Optical properties

Optical absorption properties: The optical absorption properties of the pristine and Cu doped TiO_2 catalysts were investigated by the comparison of the UV-vis diffuse reflectance spectra (DRS) as shown in Figure S4A. And it was observed that increase in Cu content brought-about shifting of absorption edge to visible light region and intense absorption, and this intense visible light absorption can be attributed to: (i) the Cu doping introduced impurity states below the conduction band minimum leading to the band gap reduction. (ii) the excitations between O 2p states and Ti 3d states through Cu 3d states. As TiO^{2+} is an indirect semiconductor, the band-gap energies of as-prepared Cu-doped TiO^2 samples estimated from the Tauc plot of $[F(R\infty)*h\nu]^{1/2}$ versus energy (E) was shown in Figure S4B. After doping of Cu^{2+} ions into TiO_2 matrix, the sample changed from white (TiO_2) to light gray. The Eg value of Cu-TiO_2 samples decrease as Cu contents increase as shown in FigureS4B, and this indicates that the samples show visible-light response.

Photodegradation of Rhodamine-B: Rhodamin-B (RhB) is one of the most commonly used organic dyes in industry and can pollute the environment. The photocatalytic activity of the Cu doped TiO_2 samples was initially evaluated by the degradation of RhB in an aqueous solution (Figure 4A). In addition, prepared mesoporous TiO_2 microspheres was used as a reference and the adsorption–desorption result of the catalyst without light irradiation showed that there was almost no change in the pollutant concentration after 60 min which indicated that an adsorption–desorption equilibrium was reached. Also, the photocatalytic degradation efficiency (PDE = $(C_0\text{-}C_t)/C_0$) of RhB hardly changed under visible light irradiation in the absence of the photocatalyst. Use of as-prepared samples for degradation of RhB shows that the photocatalytic activity of all Cu-TiO_2 samples outperformed TiO_2 sample, and TiO_2:(0.1 at% Cu) sample was the best one of them. Figure 4B shows representative variations in the absorption of RhB (λ_{max} = 554 nm) under visible light irradiation for

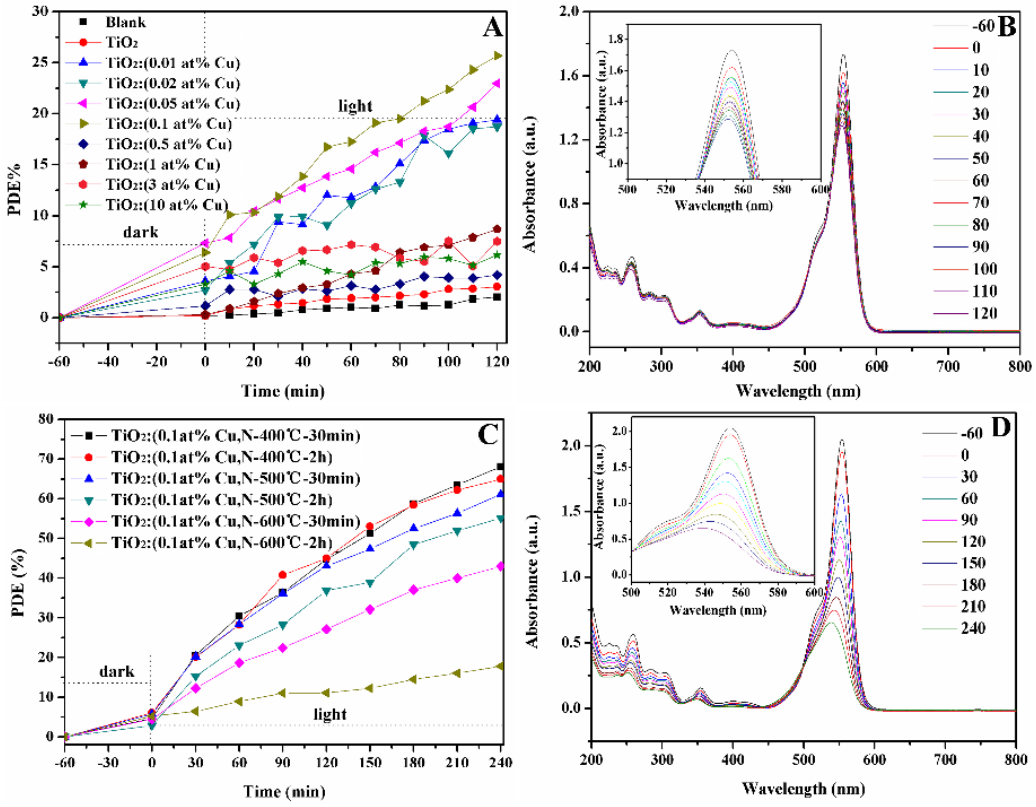

Figure 4. Time-dependent photocatalytic degradation of RhB (A) solution upon exposure to visible light using the obtained Cu-TiO_2 samples, Representative variations of the characteristic absorption of RhB (B) under visible light irradiation by using TiO_2:(0.1 at% Cu) sample (-60 to 0 as absorb time, 0-120 as photocatalysis time). Time-dependent photocatalytic degradation of RhB (C) solution upon exposure to visible light using the obtained Cu-N-TiO_2 samples, Representative variations of the characteristic absorption of RhB (D) under visible light irradiation by using TiO_2: (0.1 at% Cu, N-400°C-30 min) (-60 to 0 as absorb time, 0-240 as photocatalysis time).

the TiO_2:(0.1 at% Cu) sample as catalyst, the characteristic absorption of RhB gradually decreases as the irradiation time increases, and the characteristic wavelength shifts to a lower wavelength (inset, Figure 4B) which indicates that RhB decomposed and new substance produced.

In order to investigate the photocatalytic activity of as-prepared samples thoroughly, a kinetic study was performed for the photodegradation process. This is fitted by using pseudo-first-order kinetics, and the linear relationship of $\ln(C/C_0)$ vs time is used to calculate apparent rate constants. The results from these fitting exercises are displayed in Table 1, and the results imply that k-values 1.82×10^{-3} min^{-1} for TiO_2:(0.1 at% Cu) sample is higher than those of the other Cu-TiO_2 samples. And this is in agreement with results that show that TiO_2:(0.1 at% Cu) sample has best photocatalytic activity.

Based on the results of photocatalytic activity, the mechanism of the photocatalysis of Cu-TiO_2 samples is discussed as follow: The dopant Cu generates an impurity level of Cu^{2+} below the conduction band of TiO_2, and the electron in the valence band may be excited to the Cu^{2+} trap level with the same amount of positively charge holes left to form electron-hole pairs during light irradiation. As a consequence of this proximity, the trapped electron in Cu^{2+} could easily be released and transferred to a neighboring surficial Ti^{4+}, and the effective charge transfer might decrease the electron-hole pair recombination rate and prolonged the lifetime of charge carriers. In addition, to maintain charge neutrality, oxygen vacancies were generated by doping of Cu^{2+} in the lattice of TiO_2 and oxygen vacancies induced visible light absorption. The recombination rate of the trapped charge carriers' increases with the dopant concentration, because the average distance between the trapping sites of the two types decreases with increasing in number of dopants confined within a particle. Besides, there might be risk of reducing number of photoactive sites in the sample with too much Cu.

In addition, the mesoporous structure of the as-prepared samples results in multiple reflections of visible light within the hole, allowing the light source to be used more efficiently, which has been reported by many researchers [27]. The high BET surface area 113.3 m^2g^{-1} of TiO_2:(0.1 at% Cu) sample may offer enough photoactive sites and promote the reaction.

In order to enhance and increase the photo reactivity of TiO_2:(0.1 at% Cu) sample by extending the visible light absorption, nitriding treatment was carried out under ammonia gas, and TiO_2:(0.1 at % Cu, N-400°C-30 min) showed best photocatalytic activity, but the copper content was too low to be determined using XPS. Therefore, TiO_2:(0.5 at %Cu, N-400°C-30 min) was used to examine the copper content in the sample, and the XPS analysis was also carried out to confirm that the N doped onto mesoporous TiO_2:(0.5 at% Cu) microsphere. Meanwhile, the N peak is not obvious in EDS due to the low content of N in TiO_2:(0.1 at% Cu, N-400°C-2 h) sample. Figure 5 shows the XPS of Ti 2p, O 1s, N 1s and Cu 2p for the as-synthesized mesoporous TiO_2:(0.5 at% Cu, N-500°C-2 h) microspheres. In Figure 5A, the XPS spectrum shows complex structure 932.7 eV for Cu $2p^{3/2}$, and 952.4 eV for Cu $2p^{1/2}$ of TiO_2:(0.5 at% Cu), and this shows that Cu was incorporated into the lattice of TiO_2. Before or after nitriding treatment the peaks of Cu 2p was almost not changed, and Figure 5B shows O 1s peaks at 530.0 and 531.8 eV, the peak at 530.0 eV was assigned to the Ti-O bonds in the TiO_2 lattice and the peak at 531.8 eV was related to the hydroxyl groups or water adsorbed on TiO_2 surfaces. After nitriding treatment, the peaks of O 1s have little changes from 531.8 eV to 531.9 eV. Figure 5C shows Ti 2p spectrum, in which two peaks are observed at 458.7 and 464.4 eV for Cu-TiO_2, which correspond to the binding energies of Ti $2p^{3/2}$ and Ti $2p^{1/2}$ levels for Ti^{4+}, and Ti^{3+} spectrum was not observed using XPS. Figure 5D is the N 1s core level spectra of co-doped TiO_2, and it was found that there were two peaks with different intensity at the bonding energies of 396.1 eV and 400.4 eV. Generally, the peak at 396.1 eV reflects the formation of N-Ti-O bonds, which indicates the substitution of N-ion for O-ion, and the XPS peak at 400.4 eV could be assigned to interstitial N in TiO_2 [28]. In line with the XPS results, the total amount of doped N was 0.75% and substitutional N was 0.27%. It was difficult to make the substitution of O for N because the ionic radius of N(1.71 Å) was much bigger compared to that of O(1.4 Å) [29]. As it was reported by our previous work, the substitutional N and interstitial N play a key role in the band gap narrowing and contributed to the visible light photocatalytic degradation of RhB.

Table 1. The k-values of the as-prepared TiO_2 and Cu-TiO_2 samples.

Catalyst	k_{RhB}(10^{-3} min^{-1})
TiO_2	--
TiO_2:(0.01 at% Cu)	1.64
TiO_2:(0.02 at% Cu)	1.44
TiO_2:(0.05 at% Cu)	1.44
TiO_2:(0.1 at% Cu)	1.82
TiO_2:(0.5 at% Cu)	0.20
TiO_2:(1 at% Cu)	0.74
TiO_2:(3 at% Cu)	0.13
TiO_2:(10 at% Cu)	0.20

In Figure S5A, the absorption spectrum of TiO_2:(0.1 at% Cu, N-400°C-30 min) and TiO_2:(0.1 at% Cu,N-400°C-2 h) samples were nearly identical, and the absorption edge in the wavelength increased to 480 nm and 500 nm as the NH_3 treatment temperature and duration increased to 500°C for 30 min and 2 h. And an add-on shoulder was imposed onto the edge of the absorption spectrum. With an increase in the nitriding temperature and duration, the color of TiO_2:(0.1 at% Cu, N-600°C-2 h) sample showed a dark green color and a higher absorption intensity produced. As shown in Figure S5B, the band gap of TiO_2:(0.1 at% Cu, N-400°C-30 min) was almost not changed compared to the one before nitriding treatment, and the Eg value of TiO_2:(0.1 at% Cu, N) samples after nitriding treatment gradually decreased with increasing in temperature and duration. As indicated by XPS analysis, there are two kinds of N doping, which are substitutional doping and interstitial doping. For the substitutional doping, N 2p states mixed with O 2p states in the valence band and improved the photoreactivity through narrowing of the inherent band gap of TiO_2 to maintain the electroneutrality. The oxygen vacancies give rise to the states below the conduction edge while the interstitial nitrogen atoms induced the local states near the conduction edge. After co-doping with Cu and N, electrons could be excited from valence band to the doping Cu^{2+} energy level and from the N 2p energy level to the conduction band. Besides, it is possible that the electrons can migrate from the N 2p energy level to the doping Cu^{2+} energy level, and as a result more photoinduced charge carriers could be effectively separated to participate in the photocatalytic process, leading to a higher photocatalytic activity than Cu-TiO_2 samples.

The photocatalytic activities of the TiO_2:(0.1 at% Cu,N) samples after nitriding treatment were evaluated by monitoring the degradation of RhB, and Figure 4C shows the degradation curve of RhB catalyzed by TiO_2:(0.1 at% Cu,N) samples. TiO_2:(0.1 at% Cu, N-400°C-30 min) sample shows a relatively highest photocatalytic activity, and the degradation efficiency reached 68% after 240 min under visible-light irradiation. Figure 4D shows representative variations in the

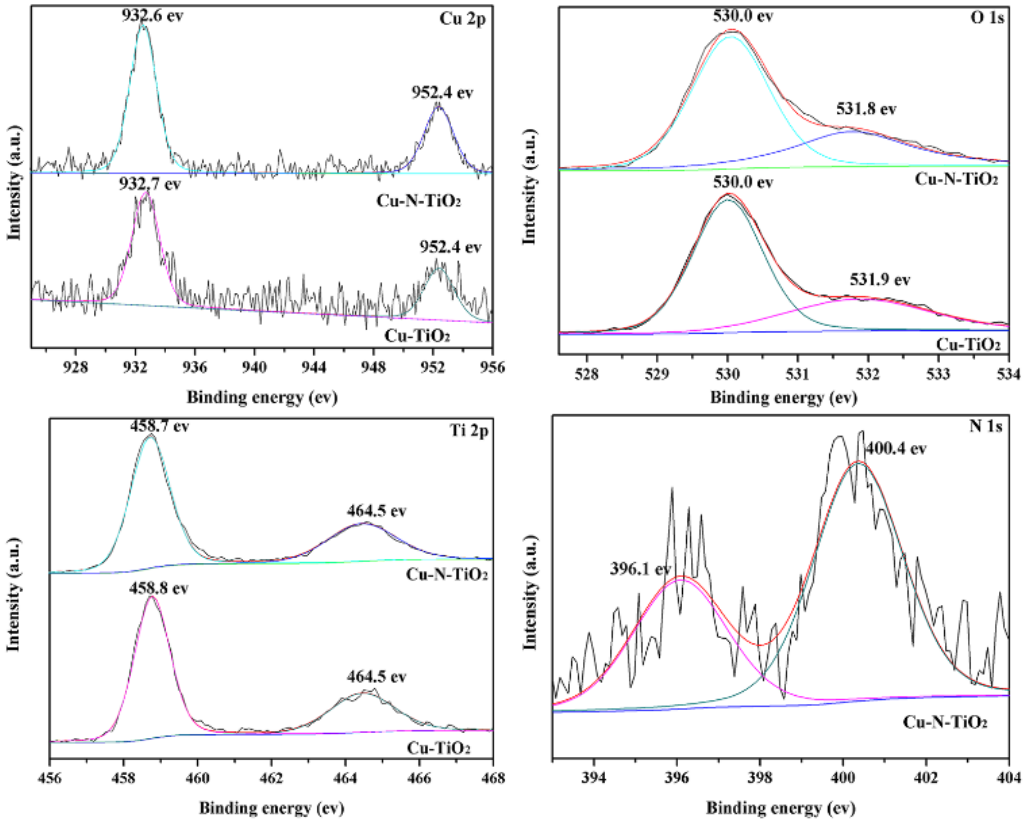

Figure 5. XPS spectra for (A) Cu (2p), (B) O(1s), (C) Ti(2p) and (D) N(1s) signals of TiO_2: (0.5 at% Cu, N-400°C-30 min).

Table 2. The k-values of the as-prepared Cu-N-TiO_2 samples.

Catalyst	$k_{RhB}(10^{-3}min^{-})$
TiO_2:(0.1 at% Cu,N - 400°C - 30 min)	4.46
TiO_2:(0.1 at% Cu,N - 400°C - 2h)	4.18
TiO_2:(0.1 at% Cu,N - 500°C - 30 min)	3.54
TiO_2:(0.1 at% Cu,N - 500°C – 2h)	3.2
TiO_2:(0.1 at% Cu,N - 600°C – 30min)	2.14
TiO_2:(0.1 at% Cu,N - 600°C - 2h)	0.56

absorption of RhB at maximum wavelength 554 nm under visible light irradiation of TiO_2:(0.1 at% Cu, N-400°C-30 min) sample. The characteristic absorption of RhB decreases obviously as the irradiation time increases, and the hypochromic shift of the maximum absorption was not obvious, indicating that a dominant cleavage of the whole conjugated chromophore structures produced instead of the N-diethylation and prolonged irradiation time might lead to the complete decomposition of RhB. Also, Figure 4C gives degradation information of RhB by TiO_2:(0.1 at% Cu, N) sample with lower values than TiO_2:(0.1 at% Cu, N-400°C-30 min) sample. At low nitriding duration and temperature, the N doped on TiO_2 mainly exists in interstitial form, and the local states near the conduction edge induce by the interstitial N (dopant) can capture electron, but this electron can be easily returned which make it impossible to narrow the band gap of TiO_2 and barely involved in the photocatalysis. Although, TiO_2:(0.1 at% Cu, N-600°C-2 h) sample absorb more visible light, but the higher density of oxygen vacancies as recombination centers lead to the decrease in the photocatalytic activity. A kinetic study was performed for the photodegradation process, and it was fitted by using pseudo-first-order kinetics, in which the value of rate constant k is equal to the corresponding slope of the fitting line. The linear relationship of $\ln(C/C_0)$ *vs.* time, and the results of TiO_2:(0.1 at% Cu, N) samples after nitriding treatment were displayed in Table 2. The results also imply that k-value for TiO_2:(0.1 at% Cu, N-400°C-30 min) sample is higher than that of TiO_2:(0.1 at% Cu, N) samples, which is in agreement with the result of photocatalytic degradation.

Conclusion

In this work, mesoporous Cu, N codoped TiO_2 photocatalysts were prepared via a solvothermal method, followed by calcination at 500°C for 2 h and nitriding treatment under ammonia gas flow. The as-prepared sample has diameter 0.60 ± 0.05 μm with relatively rough surfaces, the BET surface area was 113.3 m^2g^{-1} and its main pore sizes is smaller than 10 nm. It was found that as-prepared mesoporous Cu, N codoped TiO_2 microspheres samples showed enhanced photocatalytic activity than pure TiO_2 under visible-light irradiation, and the higher photocatalytic activity of the mesoporous Cu, N codoped TiO_2 microspheres sample could be attributed to the synergistic effects of the large BET surface area, extended light absorption, efficient charge separation, which stabilized by the presence of oxygen vacancies. From these results, we confirmed that mesoporous Cu, N codoped TiO_2 microspheres could be used to promote photodegradation of Rhodamine-B under visible light irradiation.

Acknowledgements

This work was supported by National Natural Science Foundation of China through grant 21471147 and Liaoning Provincial Natural Science Foundation through grant 2014020087. M. Yang would like to thank the National "Thousand Youth Talents" program of China.

References

1. Xin G, Pan H, Chen D, Zhang Z, Wen B (2013) Synthesis and photocatalytic activity of N-doped TiO2 produced in a solid phase reaction. *J Phys Chem Solids* 74: 286-290.
2. Salvador A, Pascual-Martí MC, Adell JR, Requeni A, March JG (2000) Analytical methodologies for atomic spectrometric determination of metallic oxides in UV sunscreen creams. *J Pharm Biomed Anal* 22: 301-306. [Crossref]
3. Moon GD, Joo JB, Dahl M, Jung H, Yin Y (2014) Nitridation and layered assembly of hollow tio2 shells for electrochemical energy storage. *Adv Funct Mater* 24: 848-856.
4. Zuo F, Wang L, Wu T, Zhang Z, Borchardt D, et al. (2010) Self-doped Ti^{3+} enhanced photocatalyst for hydrogen production under visible light. *J Am Chem Soc* 132: 11856-11857. [Crossref]
5. Bao SJ, Li CM, Zang JF, Cui XQ, Qiao Y, Guo J, et al. (2008) New nanostructured TiO_2 for direct electrochemistry and glucose sensor applications. *Adv Funct Mater* 18: 591-599.
6. Hara K, Dan-oh Y, Kasada C, Ohga Y, Shinpo A, et al. (2004) Effect of additives on the photovoltaic performance of coumarin-dye-sensitized nanocrystalline TiO_2 solar cells. *Langmuir* 20: 4205-10. [Crossref]
7. Khalid NR, Ahmed E, Hong Z, Ahmad M, Zhang Y, et al. (2013) Cu-doped TiO_2 nanoparticles/graphene composites for efficient visible-light photocatalysis. *Ceramics International* 39: 7107-13.
8. Chiarello GL, Aguirre MH, Selli E (2010) Hydrogen production by photocatalytic steam reforming of methanol on noble metal-modified TiO_2. *J Catal* 273: 182-90.
9. Guo H, Kemell M, Heikkilä M, Leskelä M (2010) Noble metal-modified TiO_2 thin film photocatalyst on porous steel fiber support. *Appl Catal B: Environ* 95: 358-364.
10. Tian B, Shao Z, Ma Y, Zhang J, Chen F (2011) Improving the visible light photocatalytic activity of mesoporous TiO_2 via the synergetic effects of B doping and Ag loading. *J Phys Chem Solids* 72: 1290-1295.
11. Choi HJ, Kang M (2007) Hydrogen production from methanol/water decomposition in a liquid photosystem using the anatase structure of Cu loaded. *Int J Hydrogen Energy* 32: 3841-3848.
12. Behnajady MA, Eskandarloo H (2013) Characterization and photocatalytic activity of Ag-Cu/TiO_2 nanoparticles prepared by sol-gel method. *J Nanosci Nanotechnol* 13: 548-553. [Crossref]
13. Liu Z, Wang Y, Peng X, Li Y, Liu Z, et al. (2012) Photoinduced superhydrophilicity of TiO_2 thin film with hierarchical Cu doping. *Sci Technol Adv Mater* 13: 025001. [Crossref]
14. Su XQ, Li J, Zhang ZQ, Yu MM, Yuan L (2015) Cu(II) porphyrins modified TiO_2 photocatalysts: Accumulated patterns of Cu(II) porphyrin molecules on the surface of TiO2 and influence on photocatalytic activity. *J Alloy Compds* 626: 252-259.
15. Sreethawong T, Yoshikawa S (2005) Comparative investigation on photocatalytic hydrogen evolution over Cu-, Pd-, and Au-loaded mesoporous TiO_2 photocatalysts. *Catal Commun* 6: 661-668.
16. Ohno T, Mitsui T, Matsumura M (2003) Photocatalytic Activity of S-doped TiO_2 Photocatalyst under Visible Light. *Chem Lett* 32: 364-365.
17. Wang J, Tafen de N, Lewis JP, Hong Z, Manivannan A, et al. (2009) Origin of photocatalytic activity of nitrogen-doped TiO_2 nanobelts. *J Am Chem Soc* 131: 12290-12297. [Crossref]
18. Sun S, Gao P, Yang Y, Yang P, Chen Y, et al. (2016) N-Doped TiO_2 Nanobelts with Coexposed (001) and (101) Facets and Their Highly Efficient Visible-Light-Driven Photocatalytic Hydrogen Production. *ACS Appl Mater Interfaces* 8: 18126-18131. [Crossref]
19. Sotelo-Vazquez C, Noor N, Kafizas A, Quesada-Cabrera R, Scanlon DO, et al. (2015) Multifunctional P-Doped TiO_2 Films: A New Approach to Self-Cleaning, Transparent Conducting Oxide Materials. *Chem Mater* 27: 3234-3242.
20. Feng H, Zhang MH, Yu LE (2013) Phosphorus-doped TiO2 catalysts with stable anatase-brookite biphase structure: synthesis and photocatalytic performance. *J Nanosci Nanotechnol* 13: 4981-4989. [Crossref]
21. Lu N, Quan X, Li J, Chen S, Yu H, et al. (2007) Fabrication of Boron-Doped TiO_2 Nanotube Array Electrode and Investigation of Its Photoelectrochemical Capability. *J Phys Chem C* 111: 11836-11842.
22. Choi H, Shin D, Yeo BC, Song T, Han SS, et al. (2016) Simultaneously Controllable Doping Sites and the Activity of a W–N Codoped TiO_2 Photocatalyst. *ACS Catal*. 6: 2745-2753.
23. Jaiswal R, Bharambe J, Patel N, Dashora A, Kothari DC, et al. (2015) Copper and Nitrogen co-doped TiO_2 photocatalyst with enhanced optical absorption and catalytic activity. *Appl Catal B: Environ*. 168-169: 333-341.
24. Song K, Zhou J, Bao J, Feng Y (2008) Photocatalytic activity of (copper, nitrogen)-codoped titanium dioxide nanoparticles. *J Am Ceram Soc* 91: 1369-1371.
25. Kong H, Huang W, Lin H, Lu H, Zhang W (2012) Effect of SnO_2-Sb2O5 Interlayer on Electrochemical Performances of a Ti-Substrate Lead Dioxide Electrode. *Chin J Chem* 30: 2059-2065.
26. Sathishkumar K, Shanmugam N, Kannadasan N, Cholan S, Viruthagiri G (2015) Synthesis and characterization of Cu^{2+} doped NiO electrode for supercapacitor application. *J Sol-Gel Sci Techn* 74: 621-630.
27. Yeh SW, Ko HH, Chiang HM, Chen YL, Lee JH, et al. (2014) Characteristics and properties of a novel in situ method of synthesizing mesoporous TiO_2 nanopowders by a simple coprecipitation process without adding surfactant. *J Alloy Compds* 613: 107-116.
28. Chong MN, Jin B, Chow CW, Saint C (2010) Recent developments in photocatalytic water treatment technology: a review. *Water Res* 44: 2997-3027. [Crossref]
29. Daghrir R, Drogui P, Robert D (2013) Modified TiO_2 for environmental photocatalytic applications: a review. *Ind Eng Chem Res* 52: 3581-3599.